



Electroweak radiative corrections to $e^+e^- \rightarrow t\bar{t}h$ at linear colliders [☆]

Yu You ^b, Wen-Gan Ma ^{a,b}, Hui Chen ^b, Ren-You Zhang ^b,
Yan-Bin Sun ^b, Hong-Sheng Hou ^b

^a CCAST (World Laboratory), P.O. Box 8730, Beijing 100080, PR China

^b Department of Modern Physics, University of Science and Technology of China (USTC), Hefei, Anhui 230027, PR China

Received 5 June 2003; received in revised form 29 July 2003; accepted 31 July 2003

Editor: T. Yanagida

Abstract

We calculate the $\mathcal{O}(\alpha_{\text{ew}})$ electroweak radiative corrections to $e^+e^- \rightarrow t\bar{t}h$ at a electron–positron linear collider (LC) in the standard model. We analyze the dependence of the $\mathcal{O}(\alpha_{\text{ew}})$ corrections on the Higgs boson mass m_h and colliding energy \sqrt{s} , and find that the corrections significantly decrease or increase the Born cross section depending on the colliding energy. The numerical results show that the $\mathcal{O}(\alpha_{\text{ew}})$ relative correction is strongly related to the Higgs boson mass when $\sqrt{s} = 500$ GeV, and for $m_h = 150$ GeV the relative correction ranges from -31.3% to 2.3% as the increment of the colliding energy from 500 GeV to 2 TeV.

© 2003 Elsevier B.V. All rights reserved.

PACS: 14.65.Ha; 14.80.Bn; 12.15.Lk; 13.66.Fg

Keywords: Higgs boson production; Electroweak radiative correction; Linear collider

1. Introduction

The main goal of the most experimental programs at present and future high-energy colliders is to search for Higgs boson, which is believed to be responsible for the breaking of the electroweak symmetry and the generation of masses for the fundamental particles in the standard model (SM) [1,2]. The fundamental particles acquire masses via the interactions with the

ground state Higgs field in the SM Higgs mechanism. However, until now the Higgs boson has not yet been directly explored experimentally, except that LEP2 experiments provided a lower bound of 114.4 GeV for the SM Higgs boson mass at the 95% confidence level [3].

As we know that the Higgs search strategies depend largely on the suspected value of Higgs mass. Actually, it is most difficult to probe Higgs boson experimentally in the intermediate mass region ($m_h \sim 100\text{--}200$ GeV). In this mass region, the production mechanism with Higgs boson radiated from either a gauge boson or a fermion, is an important Higgs

[☆] Supported by National Natural Science Foundation of China.
E-mail address: youyu@mail.ustc.edu.cn (Y. You).

boson discovery channel. At e^+e^- linear colliders and hadron colliders, the Higgs boson is searched via Bjorken process $e^+e^-(p\bar{p}, pp) \rightarrow f\bar{f}h$, an intermediate Higgs boson is produced associated with a $f\bar{f}$ pair. The coupling strength of the fermion–Higgs Yukawa coupling $f\bar{f}h$ is proportional to the fermion mass, i.e., $g_{f\bar{f}h} = m_f/v$, where $v = (\sqrt{2}G_F)^{-1/2} \simeq 246$ GeV is the vacuum expectation value of the Higgs boson. Then we can see that the top quark Yukawa coupling $g_{t\bar{t}h}$ is the largest one among all the fermion–Higgs couplings, e.g., $g_{t\bar{t}h}^2 \simeq 0.5$ to be compared for example with $g_{b\bar{b}h}^2 \simeq 4 \times 10^{-4}$. Therefore, the Higgs boson production via the process $e^+e^- \rightarrow t\bar{t}h$ is strongly enhanced by the top quark Yukawa coupling, and it can also be a basic mechanism for measuring the top quark Yukawa coupling.

Recently, a lot of efforts have been invested in improving the precise QCD theoretical corrections to the processes $p\bar{p}/pp \rightarrow t\bar{t}h + X$ [4–8]. At a LC the cross section for $e^+e^- \rightarrow t\bar{t}h$ is small, about 1 fb for $\sqrt{s} = 500$ GeV and $m_h = 100$ GeV [9–11]. But it has a distinctive experimental signature and can potentially be used to measure the top quark Yukawa coupling in the intermediate Higgs mass region at a LC with very high luminosity. In Ref. [10], Dawson and Reina found that the NLO QCD corrections increase the Born cross section by a factor of roughly 1.5 for $e^+e^- \rightarrow t\bar{t}h$ at $\sqrt{s} = 500$ GeV and $m_h = 100$ GeV. But at $\sqrt{s} = 1$ TeV, the corrections decrease the Born cross section and are relative small. These works show that the evaluation of radiative corrections is a crucial task for all accurate measurements of this process.

In this Letter we present the calculations of the full $\mathcal{O}(\alpha_{\text{ew}})$ electroweak corrections to $e^+e^- \rightarrow t\bar{t}h$ in the SM. In Section 2, we present our calculations of the full $\mathcal{O}(\alpha_{\text{ew}})$ electroweak radiative corrections. The numerical results and discussions are presented in Section 3. Finally, a short summary is given.

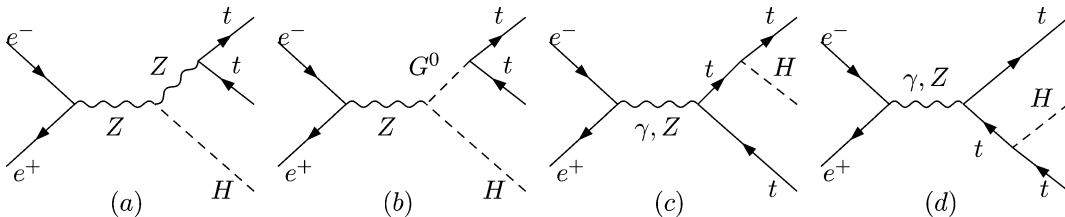


Fig. 1. The tree-level Feynman diagrams for the $e^+e^- \rightarrow t\bar{t}h$ process.

2. Calculations

In this Letter we use the 't Hooft–Feynman gauge. In the calculations of loop diagrams we adopt the definitions of one-loop integral functions of Ref. [15]. The Feynman diagrams and the relevant amplitudes are created by *FeynArts* 3 [16] automatically, and the Feynman amplitudes are subsequently reduced by *FORM* [17]. The numerical calculations of integral functions are implemented by using Fortran programs, in which the 5-point loop integrals are evaluated by using the approach presented in Ref. [13].

The process $e^+e^- \rightarrow t\bar{t}h$ at the lowest level occurs through the Feynman diagrams of Fig. 1. There are two kinds of Feynman diagrams to the $e^+e^- \rightarrow t\bar{t}h$ process at the tree-level. The first kind includes diagrams with Higgsstrahlungs from top or anti-top final states and the top Yukawa coupling is thus involved. The second kind consists of the diagrams with a Higgs boson radiated from a Z^0 -exchange s -channel or via Z^0 – G^0 – h interaction, and is independent of the top Yukawa coupling. We have checked that our numerical Born cross section is in good agreement with that in Refs. [10,12,14].

The $\mathcal{O}(\alpha_{\text{ew}})$ (one-loop level) virtual corrections to the process

$$e^+(p_1) + e^-(p_2) \rightarrow t(k_1) + \bar{t}(k_2) + h(k_3) \quad (2.1)$$

can be expressed as

$$\begin{aligned} \sigma_{\text{virtual}} &= \sigma_0 \delta_{\text{virtual}} \\ &= \frac{N_c}{2|k_1|\sqrt{s}} \int d\Phi_3 \sum_{\text{spin}} \text{Re}(\mathcal{M}_0 \mathcal{M}_{\text{virtual}}^*), \end{aligned} \quad (2.2)$$

where σ_0 and \mathcal{M}_0 are the Born cross section and amplitude for $e^+e^- \rightarrow t\bar{t}h$, respectively, $d\Phi_3$ is the three-body phase space element, the bar over summation recalls averaging over initial spins, and $\mathcal{M}_{\text{virtual}}$

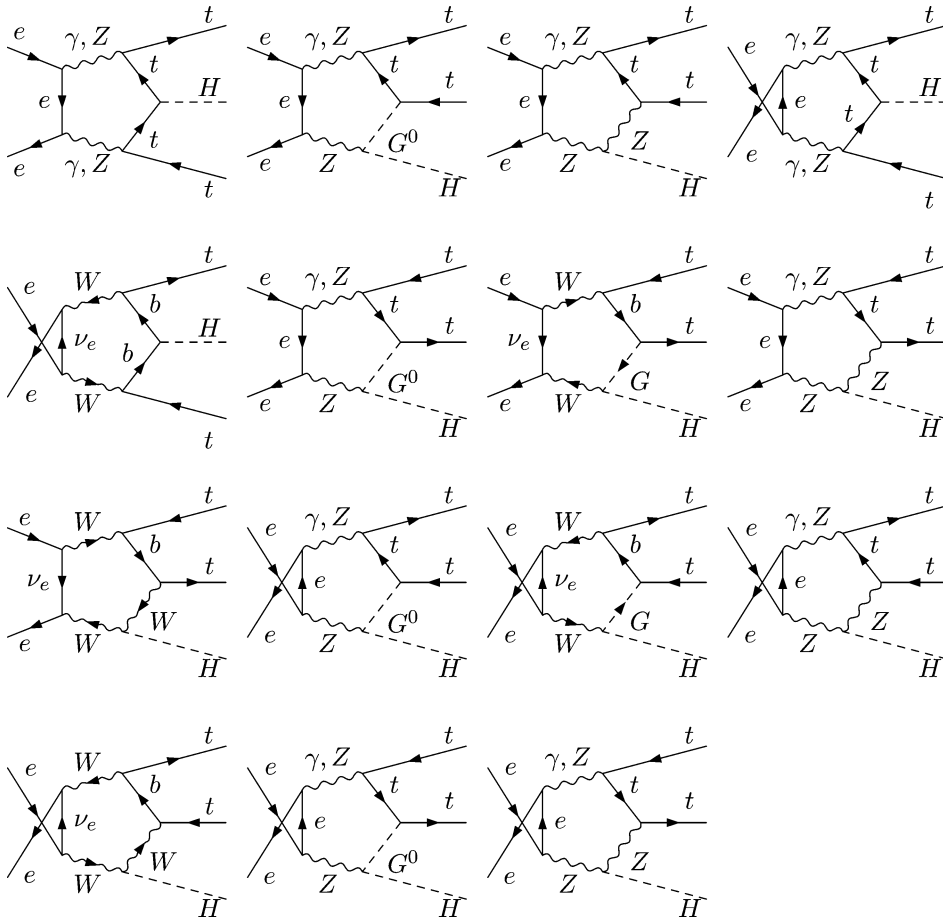


Fig. 2. The pentagon diagrams for the $e^+e^- \rightarrow t\bar{t}h$ process.

is the amplitude of one-loop Feynman diagrams and the corresponding counter-terms. Due to the fact that the electron–Higgs (Goldstone) Yukawa coupling is proportional to the electron mass, we do not consider the contributions of the one-loop diagrams which involve $\bar{e}-e-h(G^0)$ vertex to the amplitude $\mathcal{M}_{\text{virtual}}$. Therefore, the $\mathcal{O}(\alpha_{\text{ew}})$ virtual corrections involve 975 loop diagrams which can be classified into self-energy (376), vertex (425), box (145) and pentagon (29) diagrams. As a representative selection, the pentagon diagrams are given in Fig. 2.

The self-energy and vertex one-loop diagrams contain both ultraviolet (UV) and infrared (IR) divergences, while all the box and pentagon diagrams are ultraviolet finite and only contain IR divergences. To regularize the UV divergences in loop integrals, we

adopt the dimensional regularization scheme [18] in which the dimensions of spinor and spacetime manifolds are extended to $D = 4 - 2\epsilon$. In this Letter, we adopt the complete on-mass-shell (COMS) renormalization scheme [19], in which the electric charge of electron e and the physical masses m_W, m_Z, m_h, m_t, m_e are chosen to be the renormalized parameters. The definitions and the explicit expressions of these renormalization constants can be found in Ref. [19]. As we expect, the UV divergence contributed by the one-loop diagrams can be cancelled by that contributed by the counterterms exactly. Therefore, we get a UV finite cross section including $\mathcal{O}(\alpha_{\text{ew}})$ virtual radiative corrections.

The IR divergence in the process $e^+e^- \rightarrow t\bar{t}h$ is originated from virtual photonic corrections. It can

be exactly cancelled by including the real photonic bremsstrahlung corrections to this process in the soft photon limit. The real photon emission process

$$e^+(p_1) + e^-(p_2) \rightarrow t(k_1) + \bar{t}(k_2) + h(k_3) + \gamma(k), \quad (2.3)$$

where the real photon radiates from the initial electron (positron) and the final top (anti-top) quark, can have either soft or collinear nature. The collinear singularity is regularized by keeping electron mass. In order to isolate the soft photon emission singularity in the real photon emission process, we use the general phase-space-slicing method [20]. The bremsstrahlung phase space is divided into singular and non-singular regions, and the cross section of the real photon emission process (2.3) is decomposed into soft and hard terms

$$\sigma_{\text{real}} = \sigma_{\text{soft}} + \sigma_{\text{hard}} = \sigma_0(\delta_{\text{soft}} + \delta_{\text{hard}}). \quad (2.4)$$

For soft photons, $k_0 < \Delta E$, we neglect the momenta of the radiated photons everywhere but in the singular propagators. By using the soft photon approximation, we find the contribution of the soft photon emission process is [19,21]

$$\begin{aligned} d\sigma_{\text{soft}} = & -d\sigma_0 \frac{\alpha_{\text{ew}}}{2\pi^2} \int_{|\vec{k}| \leq \Delta E} \frac{d^3k}{2k_0} \\ & \times \left[\frac{Q_e p_1}{p_1 \cdot k} - \frac{Q_e p_2}{p_2 \cdot k} - \frac{Q_t k_1}{k_1 \cdot k} + \frac{Q_t k_2}{k_2 \cdot k} \right]^2, \end{aligned} \quad (2.5)$$

in which ΔE is the energy cutoff of the soft photon and $k_0 \leq \Delta E \ll \sqrt{s}$, $Q_e = 1$ and $Q_t = 2/3$ are the electric charges of the positron and top quark. $k_0 = \sqrt{|\vec{k}|^2 + \mu^2}$ is the photon energy. The integral over the soft photon phase space have been implemented, therefore, we obtain the analytical result of the soft corrections to $e^+e^- \rightarrow t\bar{t}h$ which can be found in Refs. [19] and [21]. We checked numerically the cancellation of IR divergencies and verified the contribution of these soft photonic bremsstrahlung corrections leads to a IR finite cross section which is independent of the infinitesimal photon mass μ . The hard photon emission cross section σ_{hard} , with the radiated photon energy being larger than ΔE , is calculated by using Monte Carlo method.

Finally the UV and IR finite total cross section including the full $\mathcal{O}(\alpha_{\text{ew}})$ electroweak corrections reads

$$\sigma = \sigma_0 + \Delta\sigma = \sigma_0 + \sigma_{\text{virtual}} + \sigma_{\text{real}} = \sigma_0(1 + \delta), \quad (2.6)$$

where $\delta = \delta_{\text{virtual}} + \delta_{\text{soft}} + \delta_{\text{hard}}$ is the full electroweak relative correction of the order $\mathcal{O}(\alpha_{\text{ew}})$.

3. Numerical results and discussions

In our numerical calculations, we set [22]: $\alpha_{\text{ew}}(0)^{-1} = 137.0359895$, $m_W = 80.423$ GeV, $m_Z = 91.188$ GeV, $m_e = 0.511$ MeV, $m_\mu = 105.7$ MeV, $m_\tau = 1.777$ GeV, $m_u = 66$ MeV, $m_c = 1.35$ GeV, $m_t = 174.3$ GeV, $m_d = 66$ MeV, $m_s = 150$ MeV, and $m_b = 4.3$ GeV. The renormalization scale is taken to be $Q = 2m_t + m_h$. Here we use the effective values of the light quark masses (m_u and m_d) which can reproduce the hadron contribution to the shift in the fine structure constant $\alpha_{\text{ew}}(m_Z)$ [23].

In Fig. 3 we show the dependence of the $\mathcal{O}(\alpha_{\text{ew}})$ relative correction to $e^+e^- \rightarrow t\bar{t}h$ on the soft cut-off $\Delta E/E_b$, assuming $m_h = 115$ GeV and $\sqrt{s} = 500$ GeV. As shown in this figure, both $\delta_{\text{virtual+soft}}$ ($= \delta_{\text{virtual}} + \delta_{\text{soft}}$) and δ_{hard} depend on the soft cut-off $\Delta E/E_b$, but the full $\mathcal{O}(\alpha_{\text{ew}})$ electroweak relative correction δ is cutoff independent within the range of

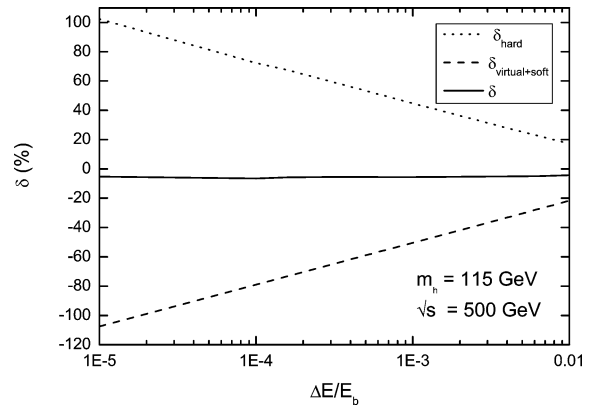


Fig. 3. The relative corrections of the $\mathcal{O}(\alpha_{\text{ew}})$ order contributions to the $e^+e^- \rightarrow t\bar{t}h$ cross section. The relative corrections of $\delta_{\text{virtual+soft}}$ and δ_{hard} , and their sum are shown as the functions of the soft photon energy cutoff $\Delta E/E_b$.

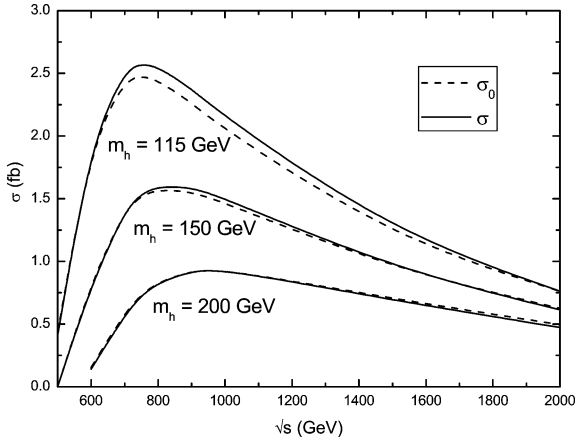


Fig. 4. The Born and one-loop level cross sections for the process $e^+e^- \rightarrow t\bar{t}h$ as functions of the e^+e^- colliding energy \sqrt{s} .

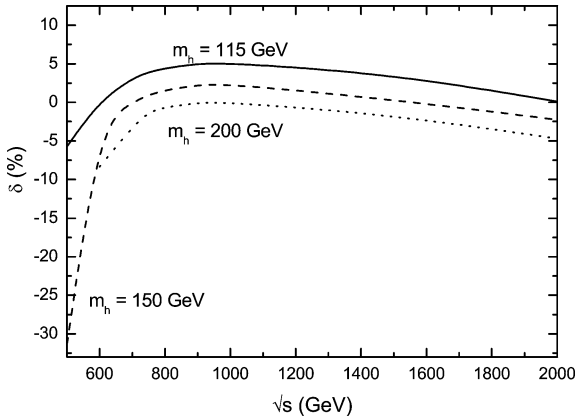


Fig. 5. The dependence of the $\mathcal{O}(\alpha_{ew})$ relative correction to $e^+e^- \rightarrow t\bar{t}h$ on the e^+e^- colliding energy \sqrt{s} .

statistical errors as expected. In the following calculations, the soft cutoff $\Delta E/E_b$ is fixed to be 10^{-3} .

In Fig. 4 we present the Born cross section σ_0 and the one-loop level cross section σ which include the full $\mathcal{O}(\alpha_{ew})$ electroweak corrections, as functions of the e^+e^- colliding energy \sqrt{s} for the Higgs boson mass $m_h = 115, 150$ and 200 GeV, respectively. The colliding energy range (500 GeV–2 TeV) in the figure is accessible at future linear colliders, such as, TESLA [24] ($\sqrt{s} = 500$ GeV), NLC [25] ($\sqrt{s} = 500$ GeV), JLC [26] ($\sqrt{s} = 500$ GeV), and CERN CLIC [27] ($1 < \sqrt{s} < 5$ TeV). From this figure we can see that both curves of σ_0 and σ for $m_h = 115$ GeV reach maximal values at the position of $\sqrt{s} \sim 750$ GeV, where the

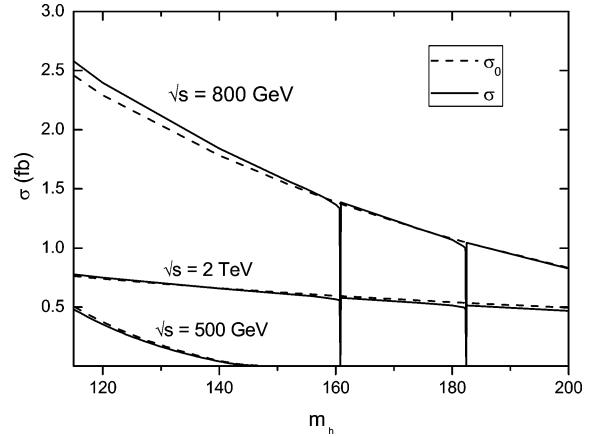


Fig. 6. The Born and one-loop level cross sections for the process $e^+e^- \rightarrow t\bar{t}h$ as functions of the Higgs boson mass m_h .

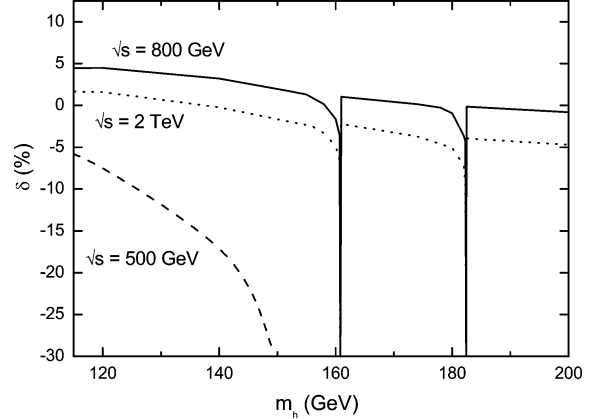


Fig. 7. The $\mathcal{O}(\alpha_{ew})$ relative correction to the process $e^+e^- \rightarrow t\bar{t}h$ as a function of the Higgs boson mass m_h .

correction $\Delta\sigma$ can reach 0.09 fb. For $m_h = 150$ GeV and 200 GeV, both σ_0 and σ have their maximal values at $\sqrt{s} \sim 850$ GeV and $\sqrt{s} \sim 950$ GeV, respectively. The correction $\Delta\sigma$ decreases as the increment of the Higgs boson mass m_h .

The dependence of the $\mathcal{O}(\alpha_{ew})$ relative correction to $e^+e^- \rightarrow t\bar{t}h$ on the colliding energy \sqrt{s} of a LC is displayed in Fig. 5. For $m_h = 115$ GeV, the $\mathcal{O}(\alpha_{ew})$ corrections suppress the Born cross section in the energy region of $\sqrt{s} < 600$ GeV, while enhance the Born cross section in the region of $\sqrt{s} > 600$ GeV. The relative corrections can reach about -5.8% , -31.3% and -8.3% at $\sqrt{s} = 500, 500$ and 600 GeV for $m_h = 115, 150$ and 200 GeV, respectively. For $m_h =$

150 GeV, the relative correction ranges from -31.3% to 2.3% as \sqrt{s} running from 500 GeV to 2 TeV. The large correction for $\sqrt{s} = 500$ GeV and $m_h \sim 150$ GeV shown in this figure comes from a threshold effect which diverges at the threshold.

In Fig. 6 we depict the Born cross section σ_0 and the one-loop level cross section σ as functions of the Higgs boson mass m_h . As shown in this figure, both the cross sections σ_0 and σ decrease with the increment of the Higgs boson mass, and the cross sections σ_0 , σ and the one-loop level correction $\Delta\sigma = \sigma - \sigma_0$ at $\sqrt{s} = 800$ GeV are larger than those at $\sqrt{s} = 500$ GeV and $\sqrt{s} = 2$ TeV.

In Fig. 7 we plot the $\mathcal{O}(\alpha_{\text{ew}})$ relative correction δ to $e^+e^- \rightarrow t\bar{t}h$ as a function of m_h . For $\sqrt{s} = 500$ GeV, the relative correction decreases from -5.8% at $m_h = 115$ GeV to -31.3% at $m_h = 150$ GeV. For $\sqrt{s} = 800$ GeV and 2 TeV, the relative corrections decrease from 4.4% and 1.5% to -0.8% and -4.7% as the increment of m_h from 115 to 200 GeV, respectively. The $\mathcal{O}(\alpha_{\text{ew}})$ electroweak relative corrections are not very sensitive to the Higgs boson mass in the range of $115 < m_h < 200$ GeV when $\sqrt{s} = 800$ GeV and 2 TeV, but strongly depend on the Higgs boson mass when $\sqrt{s} = 500$ GeV. In both Fig. 6 and Fig. 7, we can see that each of the two curves of the total cross sections including the $\mathcal{O}(\alpha_{\text{ew}})$ corrections at $\sqrt{s} = 800$ GeV and 2 TeV, has two spikes at the vicinities of $m_h = 2m_W$ and $m_h = 2m_Z$, due to the threshold effects.

After submitting this manuscript, we acknowledged another two papers appeared on this subject [28,29]. The representative comparison with the calculation of Ref. [29] is shown in Table 2 of [29]. (There we use the current mass values for m_u and m_d .) It shows that most of our numerical results of one-loop electroweak corrected cross sections agree with theirs within estimated error, but there are some discrepancies at the energy $\sqrt{s} = 2$ TeV.

4. Summary

In this Letter we calculate the full electroweak one-loop level radiative corrections to the process $e^+e^- \rightarrow t\bar{t}h$ at a electron–positron LC in the standard model. We analyze the dependence of the electroweak radiative corrections on the Higgs boson mass m_h

and colliding energy \sqrt{s} , and find that the corrections increase or decrease the Born cross section in the Higgs boson mass range $115 < m_h < 200$ GeV, depending on the colliding energy. The numerical results show that the $\mathcal{O}(\alpha_{\text{ew}})$ electroweak relative corrections can reach -31.3% , 4.4% and -4.7% at $\sqrt{s} = 500$, 800 GeV and 2 TeV, respectively. We also find that the full electroweak relative correction of the order $\mathcal{O}(\alpha_{\text{ew}})$ is strongly related to the Higgs boson mass when $\sqrt{s} = 500$ GeV, and for $m_h = 150$ GeV the relative correction ranges from -31.3% to 2.3% as the colliding energy increasing from 500 GeV to 2 TeV.

Acknowledgements

This work was supported in part by the National Natural Science Foundation of China and a grant from the University of Science and Technology of China.

References

- [1] S.L. Glashow, Nucl. Phys. 22 (1961) 579; S. Weinberg, Phys. Rev. Lett. 1 (1967) 1264; A. Salam, in: N. Svartholm (Ed.), Proceedings of the 8th Nobel Symposium, Stockholm 1968, Almquist and Wiksells, Stockholm, 1968, p. 367; H.D. Politzer, Phys. Rep. 14 (1974) 129.
- [2] P.W. Higgs, Phys. Lett. 12 (1964) 132; P.W. Higgs, Phys. Rev. Lett. 13 (1964) 508; P.W. Higgs, Phys. Rev. 145 (1966) 1156; F. Englert, R. Brout, Phys. Rev. Lett. 13 (1964) 321; G.S. Guralnik, C.R. Hagen, T.W.B. Kibble, Phys. Rev. Lett. 13 (1964) 585; T.W.B. Kibble, Phys. Rev. 155 (1967) 1554.
- [3] ALEPH, DELPHI, L3 and OPAL Collaborations, The LEP Working Group for Higgs Boson Search, LHWG note 2002-01, July, 2002, contributed paper for ICHEP'02, Amsterdam, July, 2002, and additional updates at <http://lephiggs.web.cern.ch/LEPHIGGS/www/Welcome.html>; P.A. McNamara, S.L. Wu, Rep. Prog. Phys. 65 (2002) 465.
- [4] L. Reina, S. Dawson, Phys. Rev. Lett. 87 (2001) 201804.
- [5] L. Reina, S. Dawson, D. Wackerroth, Phys. Rev. D 65 (2002) 053017.
- [6] W. Beenakker, S. Dittmaier, M. Krämer, B. Plümer, M. Spira, P.M. Zerwas, Phys. Rev. Lett. 87 (2001) 201805; W. Beenakker, S. Dittmaier, M. Krämer, B. Plümer, M. Spira, P.M. Zerwas, Nucl. Phys. B 653 (2003) 151.
- [7] D. Rainwater, M. Spira, D. Zeppenfeld, MAD-PH-02-1260, hep-ph/0203187.
- [8] J. Goldstein, C.S. Hill, J. Incandela, S. Parke, D. Rainwater, D. Stuart, Phys. Rev. Lett. 86 (2001) 1694.

- [9] S. Dittmaier, M. Krämer, Y. Liao, M. Spira, P.M. Zerwas, Phys. Lett. B 441 (1998) 383.
- [10] S. Dawson, L. Reina, Phys. Rev. D 59 (1999) 054012.
- [11] A. Juste, G. Merino, hep-ph/9910301.
- [12] A. Djouadi, J. Kalinowski, P.M. Zerwas, Mod. Phys. Lett. A 7 (1992) 1765;
A. Djouadi, J. Kalinowski, P.M. Zerwas, Z. Phys. C 54 (1992) 255.
- [13] A. Denner, S. Dittmaier, Nucl. Phys. B 658 (2003) 175.
- [14] K.J.F. Gaemers, G.J. Gounaris, Phys. Lett. B 77 (1978) 379.
- [15] G. Passarino, M. Veltman, Nucl. Phys. B 160 (1979) 151.
- [16] T. Hahn, Comput. Phys. Commun. 140 (2001) 418.
- [17] J.A.M. Vermaseren, math-ph/0010025.
- [18] G. 't Hooft, M. Veltman, Nucl. Phys. B 44 (1972) 189.
- [19] A. Denner, Fortschr. Phys. 41 (1993) 307.
- [20] W.T. Giele, E.W. Glover, Phys. Rev. D 46 (1992) 1980;
W.T. Giele, E.W. Glover, D.A. Kosower, Nucl. Phys. B 403 (1993) 633;
S. Keller, E. Laenen, Phys. Rev. D 59 (1999) 114004.
- [21] G. 't Hooft, M. Veltman, Nucl. Phys. B 153 (1979) 365.
- [22] K. Hagiwara, et al., Phys. Rev. D 66 (2002) 1.
- [23] F. Legerlehner, DESY-01-029, hep-ph/0105283.
- [24] R. Brinkmann, K. Flottmann, J. Rossbach, P. Schmuser, N. Walker, H. Weise (editor), TESLA: The superconducting electron positron linear collider with an integrated X-ray laser laboratory. Technical design report, Part 2: The Accelerator, DESY-01-11, March, 2001.
- [25] C. Adolphsen, et al., International Study Group Collaboration, International study group progress report on linear collider development, SLAC-R-559 and KEK-REPORT-2000-7, April, 2000.
- [26] N. Akasaka, et al., JLC design study, KEK-REPORT-97-1.
- [27] G. Guignard (Ed.), A 3 TeV e^+e^- linear collider based on CLIC technology, CERN-2000-008.
- [28] G. Belanger, et al., LAPH-986, KEK-CP-141, KEK-TH-892, hep-ph/0307029.
- [29] A. Denner, S. Dittmaier, et al., KA-TP-05-2003, MPP-2003-27, PSI-PR-03-12, hep-ph/0307193.